fractal and fractional

MDPI

Article

Detrended Fluctuation Analysis Complements Spectral Features in Characterizing Functional Brain Aging

Simone Cauzzo [1,2], Sadaf Moaveninejad [1], Angelo Antonini [2,3], Maurizio Corbetta [3,4,5] and Camillo Porcaro [1,3,6,7,*]

1 Biomedical Engineering Research to Advance and Innovate Translational Neuroscience (BRAIN Unit), Department of Neuroscience, University of Padova, 35122 Padova, Italy; simone.cauzzo@unipd.it (S.C.)
2 Parkinson Disease and Movement Disorders Unit, Center for Rare Neurological Diseases (ERN-END), Department of Neuroscience, University of Padova, 35122 Padova, Italy
3 Department of Neuroscience and Padova Neuroscience Center, University of Padova, 35122 Padova, Italy
4 Veneto Institute of Molecular Medicine (VIMM), 35129 Padova, Italy
5 Azienda Ospedaliera University of Padova, 35122 Padova, Italy
6 Institute of Cognitive Sciences and Technologies (ISTC)-National Research Council (CNR), 00196 Rome, Italy
7 Centre for Human Brain Health and School of Psychology, University of Birmingham, Birmingham B15 2TT, UK
* Correspondence: camillo.porcaro@unipd.it

Abstract

Aging is a significant risk factor for several neurodegenerative diseases. Understanding brain aging processes is a fundamental step in identifying the early signs of pathological dysfunction. Nonetheless, regional functional changes are still poorly characterized. In this study, we employed Detrended Fluctuation Analysis (DFA) to investigate age-related changes in the scale-free temporal dynamics of blood oxygen level-dependent (BOLD) signal fluctuations derived from resting-state networks. We compared DFA to fractional amplitude of low-frequency fluctuations (fALFF) to assess their ability to discriminate between young and old adults. Significant decreases ($p < 0.01$) in fALFF in the visuospatial and dorsal default mode networks and in DFA in the salience network, were identified as key predictors of functional brain aging. Using machine learning, we showed that DFA and fALFF provide complementary information for predicting aging, with an accuracy of approximately 80% achieved only through their combined use. Overall, DFA captures alterations in scale-free temporal organization that complement conventional spectral measures, providing additional insight into network-specific functional aging.

Keywords: aging; resting-state; scale-free dynamics; detrended fluctuation analysis; functional MRI

Academic Editor: Carlo Cattani

Received: 6 January 2026
Revised: 12 February 2026
Accepted: 25 March 2026
Published: 27 March 2026

1. Introduction

Aging is a multifaceted process that increases the risk of developing neurodegenerative diseases. Beyond macroscopic atrophy, aging is increasingly understood as a progressive dysregulation of large-scale neural dynamics, affecting how distributed brain networks integrate information over time. At the biological level, these changes reflect alterations in synaptic efficacy, dendritic arborization, neuromodulatory tone, and myelin integrity, all of which influence the temporal structure of neural signaling and its hemodynamic correlates. Due to its impact on dendritic spines, synaptic density, and myelinated fibers, researchers have progressively shifted their focus from purely morphological descriptors toward models of neuronal function and connectivity [1]. This transition reflects growing evidence that age-related cognitive decline emerges from altered temporal coordination

within and between resting-state networks (RSNs), rather than from isolated regional dysfunction. BOLD signal fluctuations are thus increasingly interpreted as indirect markers of underlying neuronal synchronization and long-range temporal dependencies [2].

In this context, scale-free analysis approaches, including methods based on long-range temporal correlations, have gained relevance as tools for quantifying neural criticality, a dynamical regime characterized by scale-free temporal fluctuations and long-range correlations that optimize information processing, flexibility, and responsiveness to external demands [3]. Theoretical and empirical studies suggest that healthy brain activity operates near criticality, while aging and neurodegeneration may induce departures from this regime, either through excessive regularization or loss of long-range temporal structure [4,5]. Importantly, critical dynamics emerge from the interaction between excitation–inhibition balance, recurrent connectivity, and neuromodulatory control, mechanisms that are all known to be affected by aging [6].

Among RSNs, the default mode network (DMN), salience network, and visuospatial network play central roles in cognition and behavior and are therefore particularly relevant to the study of aging. The DMN, a major integrative hub with high metabolic demand, is thought to rely strongly on critical dynamics to support internal mentation, memory, and self-referential processing. Age-related alterations in DMN function have been consistently reported and are often interpreted as early markers of pathological vulnerability [7,8]. From a criticality perspective, changes in DMN scale-free temporal organization may reflect a loss of dynamical flexibility and reduced capacity to integrate information across temporal scales.

The salience network, which mediates the detection of behaviorally relevant stimuli and orchestrates switching between the DMN and executive networks, is increasingly recognized as a key locus of age-related change. Because this network operates at the interface between internal and external processing, it may be especially sensitive to alterations in temporal complexity and scaling behavior. Consistent with this view, abnormal temporal dynamics in salience-related circuits have been associated with impaired cognitive control and behavioral regulation in aging and disease [9]. However, despite its central functional role, the salience network has received comparatively less attention in aging studies, particularly with respect to scale-free or criticality-based metrics.

The visuospatial network, by contrast, is more directly anchored to sensory processing and exhibits strong coupling with subcortical structures. Age-related changes in this network are often robustly captured by spectral measures such as fALFF, suggesting that alterations in oscillatory power may dominate over changes in long-range temporal dependencies. This distinction makes the visuospatial network an ideal benchmark for assessing the complementary sensitivity of spectral and scale-free measures.

In recent years, metrics capturing scale-free temporal organization (e.g., DFA scaling exponents) of blood oxygen level-dependent (BOLD) time series have been increasingly used to characterize both physiological [10] and pathological brain states [9–13]. These approaches summarize alterations in local signal variability and temporal structure using univariate measures that capture defining properties of critical systems, such as power-law scaling and scale-free persistence [14]. Among the available methods to estimate scale-free dynamics, Detrended Fluctuation Analysis (DFA) is among the most widely used approaches for quantifying power-law scaling in scale-free processes [15], as it captures long-range temporal correlations in non-stationary signals and does not require signal stationarity, making it particularly suitable for resting-state fMRI where slow drifts and low-frequency, nonstationary fluctuations are intrinsic to BOLD time series [16].

A growing body of evidence indicates that spontaneous neural activity exhibits scale-free temporal organization, characterized by long-range temporal correlations and power-

law scaling behavior. These properties are widely interpreted as being consistent with fractal-like dynamics emerging from complex interactions within large-scale brain networks. This scale-free organization is consistent with theoretical models of brain activity operating near a critical regime, where neural systems maximize information processing capacity and dynamical flexibility.

In this study, fractal dimension and DFA-derived scaling exponents are interpreted as empirical measures of scale-free temporal organization and long-range correlations, rather than as strict mathematical proofs of fractality.

Early work by Linkenkaer-Hansen et al. [17] demonstrated that human brain oscillations display long-range temporal correlations spanning several time scales, providing empirical evidence for scale-free dynamics in electrophysiological signals. Subsequent studies have extended these findings to large-scale brain activity measured with functional neuroimaging. In particular, He et al. [18] showed that spontaneous brain activity exhibits scale-invariant temporal structure, consistent with fractal dynamics arising from network interactions across multiple spatial and temporal scales. Similarly, Expert et al. [19] demonstrated that resting-state fMRI signals display scale-free temporal dynamics, suggesting that brain activity operates near a critical regime characterized by self-similar fluctuations.

Within this theoretical framework, Detrended Fluctuation Analysis (DFA) has become one of the most widely used methods for quantifying long-range temporal correlations in non-stationary physiological signals. DFA estimates a scaling exponent that reflects the persistence of temporal fluctuations across time scales, providing a robust measure of scale-free temporal organization. Previous work has shown that DFA-derived scaling exponents are closely related to scale-free temporal properties of neural activity and to the intrinsic complexity of brain dynamics [20].

Importantly, the presence of a scaling exponent should not be interpreted as a strict mathematical proof of fractal structure, but rather as an empirical indicator of scale-free temporal organization. DFA therefore provides a well-established framework for detecting long-range temporal correlations and scale-invariant behavior in complex biological systems. In neuroscience, such scaling properties are widely interpreted as signatures of scale-free neural dynamics emerging from the collective activity of large-scale brain networks operating near criticality, a regime thought to optimize information processing and adaptability [5,21]. In the present study, DFA is therefore employed not as a simple power-law fitting procedure but as a quantitative measure of scale-free neural dynamics, enabling the characterization of how these properties vary across resting-state networks and across the human lifespan.

However, it remains debated whether DFA captures information beyond that provided by classical spectral measures [22]. Fractional amplitude of low-frequency fluctuations (fALFF), for example, is a widely adopted univariate spectral feature that quantifies the relative contribution of low-frequency oscillations to the overall BOLD signal and has been extensively linked to aging and neurodegenerative processes [23]. While fALFF is sensitive to changes in oscillatory power, it does not explicitly characterize temporal correlations across scales, which are central to the notion of criticality. As a result, spectral and scale-free measures may capture distinct, and potentially complementary, facets of functional brain aging.

Although DFA has been applied to aging and disease-related changes in brain dynamics, most prior studies have focused either on global signals or on isolated regions. To our knowledge, a systematic, network-specific comparison of DFA and fALFF across multiple RSNs, and their joint use in predictive models of brain aging, has not yet been performed. Regarding novelty, we now clarify that: (i) prior studies [24] demonstrated age-related changes in scale-free temporal dynamics (often interpreted as fractal-like behavior), pri-

marily in EEG and MEG; (ii) our study extends this approach to network-specific BOLD dynamics, linking DFA and fALFF metrics to predictive machine learning models of brain age, which provides mechanistic insight into RSN-specific functional aging.

In this work, we adopt a conceptual framework in which functional brain aging is viewed as a network-specific reconfiguration of critical dynamics. Under this framework, different RSNs are expected to exhibit distinct aging trajectories depending on their functional role, connectivity profile, and reliance on long-range temporal coordination. Specifically, we hypothesize that: (i) highly integrative networks such as the DMN will show pronounced changes in scale-free behavior, reflecting altered criticality and network decoupling; (ii) control and switching networks such as the salience network will be particularly sensitive to changes in detrended fluctuation properties; and (iii) sensory-dominant networks, such as the visuospatial network, will primarily exhibit aging effects captured by spectral measures like fALFF.

Within this framework, DFA and fALFF are not competing metrics but complementary descriptors of aging-related functional reorganization. The choice of DFA detrending order is therefore not merely methodological, but functionally meaningful, as it may emphasize different temporal regimes relevant to distinct RSNs.

Building on recent advances in brain-age modeling, we integrate DFA- and fALFF-derived features into a machine learning framework to assess their predictive value for estimating chronological age [9]. By combining network-specific spectral and scale-free temporal markers, we test whether criticality-informed features improve brain-age prediction beyond single-metric approaches.

In this context, the present study systematically compares DFA and fALFF in their sensitivity to age-related changes across RSNs, with a specific focus on DMN, salience, and visuospatial networks. We further investigate the impact of DFA detrending order and assess the complementarity of scale-free and spectral measures using a machine learning framework. By explicitly linking criticality-based metrics to well-characterized RSNs, our goal is to provide a mechanistic interpretation of functional brain aging and to identify network-specific markers with potential translational relevance for the early detection of neurodegenerative processes.

2. Materials and Methods

We use the dataset published by the Cambridge Center for Aging and Neuroscience (Cam-CAN), which includes pre-processed functional MRI data acquired from healthy volunteers. Subjects were instructed to keep their eyes closed, and single-run 8′:40″-long acquisitions were performed during resting state. The dataset also includes information on age, sex, handedness of subjects, and scores achieved at several behavioral and cognitive tests [25], and is subdivided into seven relatively balanced cohorts defined by age decades. All the details on inclusion/exclusion criteria can be found on the Cam-CAN Data Repository (https://cam-can.mrc-cbu.cam.ac.uk/dataset/, accessed on 6 March 2024). Data analyzed include a cohort of 61 young adults (YA, age evenly distributed between 18 and 28 years, 27 females, 34 males) and a cohort of 99 old adults (OA, age evenly distributed between 58 and 68 years, 51 females, 48 males). Chosen cohorts capture two distinct phases of adult brain function: early adulthood, when brain maturation is largely complete and cognitive function peaks; and late adulthood, when age-related neurofunctional decline becomes more consistent. These ranges enable us to compare two distinct groups and minimize the confounding effects of gradual transitions that occur in midlife.

We apply group-independent component analysis (GICA) to preprocessed functional magnetic resonance imaging data using the GIFT toolbox (v4.0.6.34) [26], based on Matlab (version 2024b, Natick, MA, USA: The MathWorks Inc.; 2024), setting the following hyper-

parameters: intensity normalization for pre-processing, standard PCA for data reduction, infomax for component estimation, and the GICA algorithm for component grouping. For each subject we use Akaike Information Criterion to define the optimal number of independent components (ICs), and the mode of this model order across subjects defines the number of sources at group level. A portion of group ICs is classified as noise by visual assessment and discarded following the indications in Griffanti et al. [27]. We select independent components (ICs) by overlapping group-level maps, Z-scored and thresholded above 2, to a set of 14 resting-state network templates [28] and by maximizing the Dice coefficient between our ICs and the templates. In IC time series back projected to the subject level, we compute fALFF using the GIFT Toolbox, and DFA using a public toolbox [29] with linear (DFA1), quadratic (DFA2), and cubic (DFA3) detrending. Specifically, given a time series $x(i)$, $i = 1, 2, \ldots, N$, the toolbox first performs mean subtraction and integration:

$$y(k) = \sum_{i=1}^{k} (x(i) - \overline{x}). \tag{1}$$

Then, the detrended, integrated signal is divided into non overlapping segments y_s of length s, and within each segment a v-order polynomial trend ${y_s}^{(v)}$ is removed and the root-mean-square fluctuation is computed as:

$$F_v^2(k) = \frac{1}{s} \sum_{k=1}^{s} \left[y((v-1)s + k) - y_s^{(v)}(k) \right]^2. \tag{2}$$

The overall fluctuation function is then computed by averaging across the number of segments N_s:

$$F(s) = \sqrt{\sum_{v=1}^{N_s} F_v^2(s)}. \tag{3}$$

F_s is plotted on a log-log scale and a scale-free (power-law) relationship is fitted:

$$F(s) \sim s^{\{a\}}, \tag{4}$$

obtaining the exponent α that is the final output.

In this work, the length of segments ranges from 8 to the total signal length, i.e., 258 volumes, with step size of 10. The effects of the group on the values of DFA1, DFA2, DFA3, and fALFF are assessed using a multivariate analysis of variance (MANOVA) and post hoc t-tests, which are corrected for false discovery rate (FDR). Before testing machine learning classifiers, we perform feature selection using the ReliefF algorithm, keeping only the best 5 components. Variance Inflation Factor (VIF) is computed on selected features to verify absence of collinearity. A 100-tree random forest classifier (RFC) implemented in Matlab is used to determine feature importance for DFA2 and fALFF across selected networks in the task of classifying YA and OA. Random Forests favor interpretability and easy feature importance evaluation while offering best accuracies in small-sized datasets and requiring minimal parameter tuning, motivating their large use in neuroimaging studies [30]. We also test the performance of a support vector machine classifier (SVMC), and of a logistic regression classifier (LRC). For all classifiers, the dataset is partitioned in 80% training and 20% test set, ensuring group stratification to maintain class balance. Hold-out training and validation is repeated 10 times using independent random-seeds stratified partitions to confirm that performance was stable across splits. For RFCs, feature importance is determined using the out-of-bag predictor importance estimates [31]. The accuracy and confusion matrices are compared between the classifier trained on mixed DFA2 and fALFF features and the classifiers trained on only one metric.

As a last step, we perform a correlation analysis between selected features and the cognitive and behavioral scores provided with the Cam-CAN dataset. For tasks providing more than two outcome scores (force matching FM, motor learning ML, reaction times RT, visual short term memory VSTM), PCA is used to reduce the outcome to two principal components. For tasks including a "total score" summary, i.e., Benton test and Cattell test, only this total score is considered. For the Hotel task, both "time" and "number of rows" scores are kept.

Calculation of DFA and fALFF, as well as all hypothesis testing and implementation of machine learning classifiers, have been performed in Matlab (The Mathworks, Inc., version R2024b).

3. Results

DFA1, DFA2, DFA3, and fALFF were computed on 14 ICs that were selected by maximizing Dice coefficients with resting-state network templates. The selected ICs were Z-scored and thresholded above two, and are shown in Figure 1 overlaid on the MNI template and divided by function, where appropriate. All four metrics showed significant group effects ($p < 0.01$, FDR corrected) for at least one IC. The post hoc Tukey–Kramer tests revealed significantly lower DFA2 values in the precuneus, the default ventral mode, the right executive control, the language and the anterior and posterior salience networks for OA. Lower fALFF values for OA were observed in the visuospatial and dorsal default mode networks. Mixed-sign differences were observed for DFA1 in the precuneus and posterior salience networks (lower for OA) and in the primary visual and dorsal default mode networks (higher for OA). The error bars in Figure 2 provide a visual indication of the differences in the values of fALFF, DFA1, DFA2 and DFA3 between YA and OA. Notably, while DFA2 obtains more significant differences than DFA1, DFA3 does not improve at all DFA2, obtaining exactly the same significant differences and in general very similar results. Given these results, we focus only on DFA2 and fALFF.

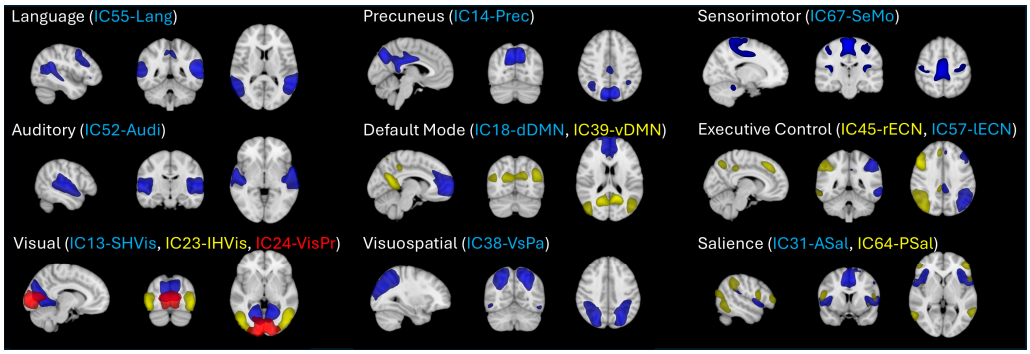

Figure 1. Maps of selected group independent components are transformed to Z-score, threhsolded above 2, and overlayed on the MNI template. Maps are presented here as binary masks, grouped by function where appropriate, and displayed with different colors to make them easily distinguishable when overlayed on a single template. Abbreviations for ICs: IC52-Audi: Auditory; IC13-SHVis: Superior High Visual; IC23-IHVis: Inferior High Visual; IC24-VisPr: Primary Visual; IC67-SeMo: Sensorimotor; IC55-Lang: Language; IC14-Prec: Precuneus; IC18-dDMN: dorsal Default Mode Network; IC39-vDMN: ventral Default Mode Network; IC38-VsPa: Visuospatial; IC45-RECN: right Executive Control; IC57-LECN: left Executive Control; IC31-ASal: Anterior Salience; IC64-PSal: Posterior Salience.

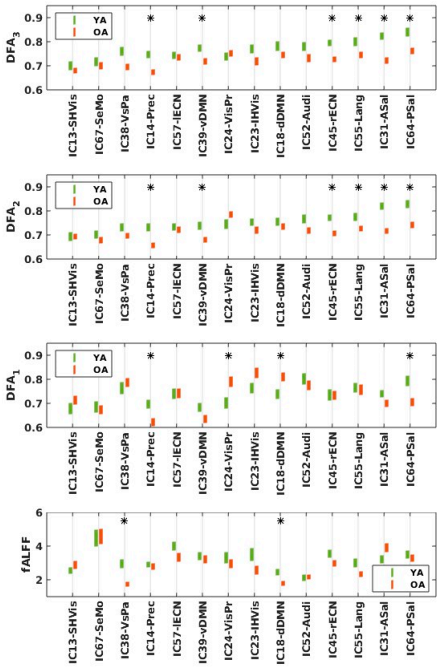

Figure 2. Differences between YA (green) and OA (red) across ICs, for (top to bottom) DFA3, DFA2, DFA1, and fALFF. Error bars represent deviations from the mean defined by standard error. Black stars on top of each panel mark significant differences, as assessed by post hoc Tukey–Kramer tests, $p < 0.05$.

We applied reliefF feature selection to the set of 14 fALFF features, obtaining as the five best performing components, in order, the superior high visual networks, the visuospatial network, the dorsal DMN, the anterior salience network and the precuneus. Feature selection performed on the set of 14 DFA2 features favored, in order, the Anterior Salience network, the primary visual network, the right executive control network, the sensorimotor network and the precuneus. Finally, selected features from the whole set of 28 are, in order, DFA2 of the anterior salience network, fALFF of the visuospatial network, fALFF of the superior high visual network, DFA2 of the primary visual network and DFA2 of the precuneus. In all three cases, feature selection granted sets of five features having variance inflation factors (VIF) below 2.2, which reasonably reports no collinearity.

In Figure 3 we report the accuracy obtained by the three classifiers across the three tasks. A RFC trained on the five mixed DFA2-fALFF features achieved 81.17 ± 4.17 percent accuracy (median ± median absolute deviation) and 27.05 ± 6.29 percent false positive rate (FPR) on the test set, while the SVMC achieved 77.00 ± 4.17 accuracy and 50.00 ± 7.89 FPR, and LRC 83.25 ± 2.08 accuracy and 31.58 ± 6.29 FPR. FPR here quantifies a consistent bias towards misclassifying OA, as demonstrated by all classifiers. The accuracies scored by the classifiers trained on mixed features improve the ones scored by classifiers using only fALFF (RFC: 73.96 ± 3.12 accuracy, 37.87 ± 4.53 FPR; SVMC: 73.96 ± 3.13 accuracy, 55.26 ± 5.56 FPR; LRC: 75.00 ± 2.08 accuracy, 48.68 ± 4.09 FPR) or only DFA2 (RFC: 69.79 ± 5.21 accuracy, 45.91 ± 7.89 FPR; SVMC: 62.50 ± 2.08 accuracy, 94.59 ± 5.41 FPR; LRC: 71.88 ± 4.17 accuracy, 51.32 ± 6.58 FPR). While all classifiers achieved highest median accuracy when using mixed DFA2-fALFF features, the difference is significant with respect to both the only-DFA2 and only-fALFF cases only for the LRC ($p < 0.05$ for both post hoc comparisons). Out-of-bag importance scores (Figure 4) computed for the RFC revealed that fALFF in the visuospatial network and DFA2 in the anterior salience network are the two most important features in classifying OA from YA. Correlations between selected features and scores obtained at the cognitive and behavioral tests are visualized in Figure 5. fALFF in the Visuospatial RSN and DFA2

in the anterior salience network are significantly correlated with the score obtained at the Cattell test, which is a test of fluid intelligence. In addition, DFA2 in the anterior salience network is also related to a first principal component of the scores obtained at the visual short term memory test (VSTM).

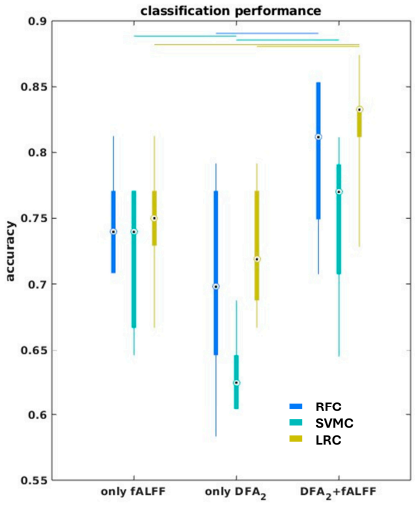

Figure 3. Accuracy obtained by three classifiers (RFC = random forest classifier, SVMC = support vector machine classifier, LRC = logistic regression classifier) on the three tasks of classifying OA from YA based on only fALFF features, only DFA2 features, or mixed DFA2 and fALFF features. Boxes represent 25% and 75% quantiles, whiskers represent total range, circles represent medians.

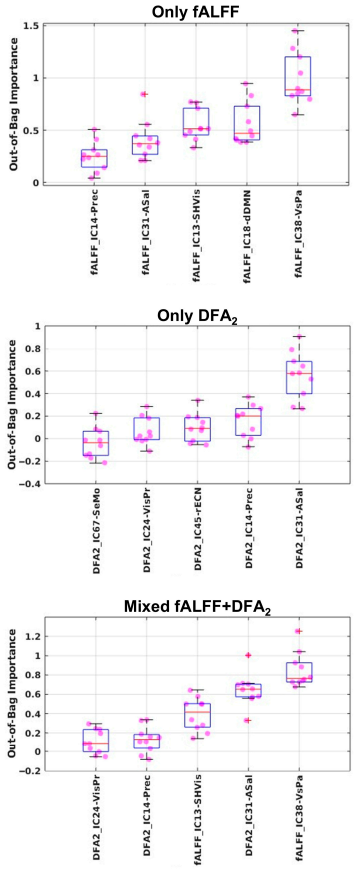

Figure 4. Feature importance as determined using the out-of-bag prediction error method. From top to bottom, importance scores obtained across the 10 subdivisions in training and test set, for fALFF features, DFA2 features, and mixed features.

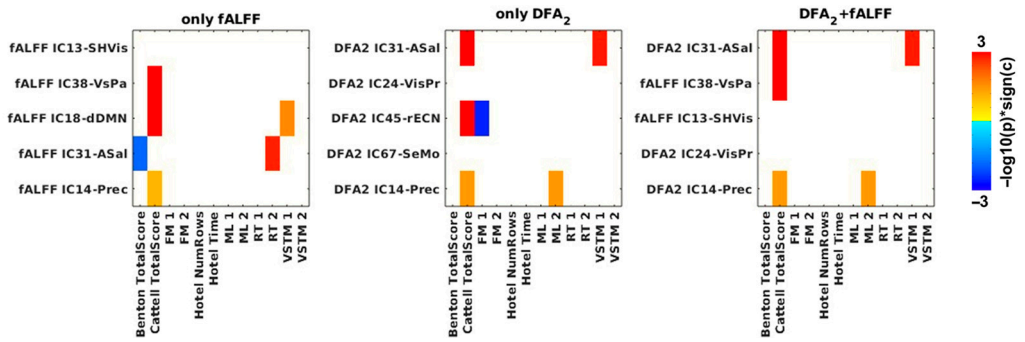

Figure 5. Correlation analysis between selected features and results obtained at cognitive and behavioral tests. Results are reported in −log10-scaled p values, multiplied by the sign of the correlation coefficient, i.e., bright red or blue means strong positive or negative correlation, respectively, while white color means that the correlation is not significant ($p < 0.05$). Abbreviations: FM = force matching, ML = motor learning, RT = reaction times, VSTM = visual short term memory.

4. Discussion

In this study, we showed that aging is associated with network-specific alterations in scale-free temporal dynamics, as quantified by Detrended Fluctuation Analysis (DFA), and that these alterations provide information complementary to conventional spectral measures such as fALFF. Specifically, DFA highlights age-related changes in higher-order cognitive networks—most prominently the salience and default mode systems—that are only partially captured by frequency-domain analyses. These findings support the view that functional brain aging involves a reorganization of critical dynamics rather than a uniform loss of activity or connectivity [32–34].

We observed that aging is a complex process that affects brain networks with different severities and modalities, and that using multiple measures in combination provides complementary information on the diverse changes that occur in functional brain networks with aging. By integrating DFA-based scale-free properties with spectral features, our results suggest that aging alters both the temporal organization of neural fluctuations and their spectral distribution, pointing to partially dissociable physiological mechanisms.

4.1. Methodological and Mechanistic Considerations on DFA

First, we present some methodological considerations regarding DFA. Here, DFA2 revealed a greater number of significant differences compared to DFA1, particularly with regard to higher-order cognitive networks (salience, executive control, ventral default mode and precuneus networks). Of these, only the differences in the posterior salience and precuneus networks are captured by DFA1. However, DFA1 captured one of the two networks for which age-related changes are most discernible using fALFF, i.e., the dorsal default mode network. This pattern suggests that DFA1 may emphasize temporal fluctuations that overlap more strongly with low-frequency spectral power, whereas DFA2 preferentially captures higher-order deviations from linear trends that reflect more complex temporal organization. On the other hand, further increases in detrending order do not seem to bring additional information, although further studies should investigate higher orders and multifractal extensions of DFA.

Importantly, DFA-derived increases or decreases in scaling exponents should not be interpreted straightforwardly as improvements or deteriorations in neural efficiency. Rather, within the framework of criticality, changes in DFA scaling likely reflect shifts in the balance between local variability and long-range temporal coordination. In the context of aging, altered DFA exponents may indicate a departure from an optimal critical regime, characterized by reduced adaptability and information integration.

While it has been suggested that discriminative power is enhanced when long-term scale-free persistence is evaluated using finely detrended data [15], here we hypothesize that different detrending strategies can highlight different types of change rather than enhancing the same observations. Thus, detrending order should not be viewed merely as a technical optimization step, but as a modeling choice that determines which physiological aspects of temporal complexity are emphasized.

This aligns with findings from multifractal analyses, in which the choice of detrending polynomial order or window size can significantly impact the identification of multifractal features. For instance, more rigorous detrending could suppress local fluctuations vital for characterizing transient or short-range dynamics, whereas less rigorous detrending could preserve these features at the expense of long-term trends. In the context of brain aging, this means that different DFA configurations (e.g., DFA1 vs. DFA2) may emphasize different aspects of temporal complexity, such as the resilience of higher-order cognitive networks or the vulnerability of core default mode regions. Therefore, rather than viewing detrending as a technical step to be optimized for maximum sensitivity, it is more appropriate to consider it as a modeling choice that determines the type of functional alterations that can be detected. This perspective is consistent with prior work on multifractal detrended fluctuation analysis (MFDFA), which has shown that different detrending regimes can reveal different multifractal spectra in physiological signals [35].

4.2. Network-Specific Aging Effects and Criticality

Figure 2 shows two main differences between DFA2 and fALFF. One difference is the distribution of baseline values across networks, which follows distinct patterns for each metric. The other difference concerns the spatial distribution of age-related effects. The effects of aging on brain function were only visible with fALFF for the visuospatial and dorsal default mode networks. These findings are consistent with the prior literature emphasizing spectral power reductions in sensory and default-mode regions, which are known early signs of brain aging [36,37].

In contrast, DFA2 revealed pronounced effects in the anterior salience network, which also achieved the second highest feature importance score in the classifier (Figure 4). The right executive control, precuneus, and ventral default mode networks showed intermediate importance. This suggests that DFA2 is particularly sensitive to age-related decline in cognitive control and long-range temporal coordination, and therefore to alterations in networks responsible for dynamic switching, attentional control, and internetwork coordination—functions that are central to maintaining near-critical dynamics.

Notably, a major improvement from the use of mixed fALFF and DFA2 features comes in terms of FPR, especially when using RFC and LRC. We observe that classifiers trained only on DFA2 features exhibit the highest FPR, which we link to the fact that DFA2 is most sensitive to age-related alterations in frontoparietal and executive networks, which are believed to occur in a later stage in life with respect to visuospatial and default-mode regions. We expect misclassifications to mainly occur for subjects whose temporal complexity patterns are preserved despite chronological aging, suggesting that DFA2 captures functional aspects of brain aging rather than purely chronological age. Nonetheless, we recognize that further studies are needed.

From a criticality perspective, the salience network plays a key role in regulating transitions between internally and externally oriented brain states. Age-related alterations in DFA scaling within this network may therefore reflect a reduced capacity to dynamically modulate large-scale brain states, consistent with behavioral observations of diminished cognitive flexibility and attentional control in older adults.

4.3. Default Mode and Visuospatial Networks: Divergent Aging Trajectories

The default mode network (DMN) showed age-related effects that differed across its subcomponents. The dorsal DMN, which is more strongly associated with cognitive control and goal-directed processes, exhibited age-related changes captured by both DFA1 and fALFF, whereas ventral components were more selectively highlighted by DFA2. This dissociation supports the notion that aging does not uniformly affect the DMN, but rather alters the balance between its subsystems.

Functionally, this decoupling may reflect a breakdown in the integration of self-referential processing and executive control, a pattern that has been associated with cognitive decline and increased vulnerability to neurodegenerative disorders. The sensitivity of DFA to these changes suggests that scale-free temporal metrics may capture early functional reorganization preceding overt structural damage.

In contrast, the visuospatial network showed prominent age-related differences primarily in fALFF. This suggests that aging-related changes in visuospatial processing may be driven more by alterations in oscillatory power and sensory integration than by changes in long-range temporal organization. The complementary sensitivity of fALFF and DFA thus reinforces the need for multimodal functional characterization.

4.4. Complementarity of DFA and Spectral Measures

Despite the classifiers trained on fALFF achieving, in general, higher accuracy than the classifiers trained solely on DFA2, the combined model outperformed both. This demonstrates that DFA and fALFF encode nonredundant information about functional aging. Spectral measures primarily capture changes in signal amplitude within predefined frequency bands, whereas DFA quantifies the temporal organization of fluctuations across scales, offering insight into critical dynamics that are not accessible through spectral analysis alone.

Notably, DFA-based features were particularly informative for networks—such as the salience network—that have received comparatively little attention in aging research [14]. This may help explain why alterations in these networks have been underreported in the literature, which has traditionally favored spectral approaches [38–41].

4.5. Translational Implications

The network-specific sensitivity of DFA to aging-related changes highlights its potential translational relevance. Alterations in DFA scaling within the salience and default mode networks may serve as early functional markers of disrupted criticality, potentially preceding measurable cognitive decline. Moreover, the non-invasive nature of resting-state fMRI combined with DFA makes this approach well suited for longitudinal monitoring and early risk stratification in aging and neurodegenerative populations.

4.6. Limitations of the Study

Despite the insights gained from the use of DFA to examine age-related changes in functional brain networks, several limitations must be acknowledged.

First, our analysis is limited to one group of YA and one of OA. This choice improves the interpretability of results, thanks to the binary nature of the classification problem, and avoids the use of subjects experiencing midlife transitions, with larger subject-specific fluctuations and possible confounds of no interest to this study such as menopause-related changes. Nonetheless, we acknowledge the need for future studies including more personal information on the status of the subject, which are not present in the Cam-CAN dataset.

Second, the interpretation of DFA results depends on the choice of the detrending order and scale range. As discussed, different DFA configurations (e.g., DFA1 vs. DFA2) can

reveal different aspects of temporal complexity, but this introduces a degree of methodological arbitrariness. Without an independent ground truth, it is difficult to determine which detrending strategy captures biologically significant changes with the most accuracy. This raises the possibility that some observed differences may reflect methodological sensitivity rather than underlying physiological alterations.

Third, while we draw connections between DFA and fALFF to infer overlapping information content, these metrics are derived from distinct mathematical frameworks and may not be directly comparable. Our suggestion that DFA1 overlaps more with fALFF requires validation through simulation studies or empirical comparisons across additional datasets.

Finally, although we examined multiple networks, our findings were based on a specific parcellation scheme and population sample. The generalizability of our results to other age groups, clinical populations, or network definitions remains to be tested. Furthermore, the absence of proper multifractal analysis (e.g., MFDFA) limits our capacity to evaluate the complete spectrum of scaling behavior in these signals, which could provide valuable insights into age-related changes in signal complexity.

5. Conclusions

In this work, we compared the power of DFA and fALFF in predicting age. We provide preliminary considerations on the optimal detrending order for DFA and using a combination of feature selection and multiple machine learning classifiers, we provide evidence for the complementarity of the two measures in capturing functional alterations related to brain aging. We conclude that second-order detrending in DFA improves linear detrending and is not further improved by higher-order detrending. Furthermore, our findings support a model in which functional brain aging is characterized by a reorganization of scale-free temporal dynamics that differs across networks, particularly across salience and visuospatial systems, and is only partially captured by spectral measures. DFA provides a complementary window into these changes, particularly in higher-order cognitive networks central to maintaining near-critical brain dynamics.

Author Contributions: Conceptualization, S.C. and C.P.; methodology, S.C. and C.P.; software, S.C. and C.P.; validation, S.C., S.M. and C.P.; formal analysis, S.C. and C.P.; investigation, C.P.; resources, C.P.; data curation, S.C. and C.P.; writing—original draft preparation, S.C. and C.P.; writing—review and editing, S.C. and C.P.; visualization, S.C. and C.P.; supervision, C.P.; project administration, M.C., A.A. and C.P.; funding acquisition, M.C., A.A. and C.P. All authors have read and agreed to the published version of the manuscript.

Funding: We acknowledge co-funding (to S.C.) from Next Generation EU, in the context of the National Recovery and Resilience Plan, Investment PE8–Project Age-It: "Ageing Well in an Ageing Society". This resource was co-financed by the Next Generation EU [DM 1557 11.10.2022]. We also acknowledge support (to M.C.) by HORIZONERC-SyG (Grant No. 101071900) "Neurological Mechanisms Of Injury And Sleep-LikeCellular Dynamics (NEMESIS)"; HORIZON-INFRA-2022 SERV (Grant No. 101147319) "EBRAINS 2.0: A Research Infrastructure to Advance Neuroscience and Brain Health". CP was supported by HORIZON-ERC-SyG (Grant No. 101071900) "Neurological Mechanisms of Injury And Sleep-Like Cellular Dynamics (NEMESIS)". This work has been partly supported by Italian PRIN Codice MUR 20228ARNXS (to C.P. and S.M.).

Institutional Review Board Statement: Not applicable.

Informed Consent Statement: Not applicable.

Data Availability Statement: Restrictions apply to the availability of these data. Data were obtained from the Cambridge Centre for Ageing and Neuroscience (Cam-CAN) and are available from the URL https://cam-can.mrc-cbu.cam.ac.uk/dataset/ upon request (accessed on 6 March 2024). Cam-

CAN funding was provided by the UK Biotechnology and Biological Sciences Research Council (grant number BB/H008217/1), together with support from the UK Medical Research Council and University of Cambridge, UK.

Conflicts of Interest: The authors declare no conflicts of interest. The funders had no role in the design of the study; in the collection, analyses, or interpretation of data; in the writing of the manuscript; or in the decision to publish the results.

Abbreviations

The following abbreviations are used in this manuscript:

BOLD	Blood-Oxygenation Level-Dependent
Cam-CAN	Cambridge Center for Aging and Neuroscience
DFA	Detrended Fluctuation Analysis
DFA1	DFA with linear detrending
DFA2	DFA with quadratic detrending
fALFF	Fractional amplitude of low frequency oscillations
GICA	Group independent component analysis
IC	Independent Component
MFDFA	Multi-fractal DFA
OA	Old Adults
PCA	Principal Component Analysis
YA	Young adults

References

1. Hou, Y.; Dan, X.; Babbar, M.; Wei, Y.; Hasselbalch, S.G.; Croteau, D.L.; Bohr, V.A. Ageing as a risk factor for neurodegenerative disease. *Nat. Rev. Neurol.* **2019**, *15*, 565–581. [CrossRef]
2. He, B.J.; Zempel, J.M.; Snyder, A.Z.; Raichle, M.E. The Temporal Structures and Functional Significance of Scale-free Brain Activity. *Neuron* **2010**, *66*, 353–369. [CrossRef]
3. O'Byrne, J.; Jerbi, K. How critical is brain criticality? *Trends Neurosci.* **2022**, *45*, 820–837. [CrossRef] [PubMed]
4. Cocchi, L.; Gollo, L.L.; Zalesky, A.; Breakspear, M. Criticality in the brain: A synthesis of neurobiology, models and cognition. *Prog. Neurobiol.* **2017**, *158*, 132–152. [CrossRef]
5. Beggs, J.M.; Plenz, D. Neuronal Avalanches in Neocortical Circuits. *J. Neurosci.* **2003**, *23*, 11167–11177. [CrossRef] [PubMed]
6. Deco, G.; Jirsa, V.K.; McIntosh, A.R. Emerging concepts for the dynamical organization of resting-state activity in the brain. *Nat. Rev. Neurosci.* **2011**, *12*, 43–56. [CrossRef]
7. Buckner, R.L.; Andrews-Hanna, J.R.; Schacter, D.L. The Brain's Default Network: Anatomy, Function, and Relevance to Disease. *Ann. N. Y. Acad. Sci.* **2008**, *1124*, 1–38. [CrossRef]
8. Andrews-Hanna, J.R.; Smallwood, J.; Spreng, R.N. The default network and self-generated thought: Component processes, dynamic control, and clinical relevance. *Ann. N. Y. Acad. Sci.* **2014**, *1316*, 29–52. [CrossRef] [PubMed]
9. Fiorenzato, E.; Moaveninejad, S.; Weis, L.; Biundo, R.; Antonini, A.; Porcaro, C. Brain Dynamics Complexity as a Signature of Cognitive Decline in Parkinson's Disease. *Mov. Disord.* **2024**, *39*, 305–317. [CrossRef]
10. Porcaro, C.; Mayhew, S.D.; Marino, M.; Mantini, D.; Bagshaw, A.P. Characterisation of Haemodynamic Activity in Resting State Networks by Fractal Analysis. *Int. J. Neural Syst.* **2020**, *30*, 2050061. [CrossRef]
11. Porcaro, C.; Di Renzo, A.; Tinelli, E.; Di Lorenzo, G.; Parisi, V.; Caramia, F.; Fiorelli, M.; Di Piero, V.; Pierelli, F.; Coppola, G. Haemodynamic activity characterization of resting state networks by fractal analysis and thalamocortical morphofunctional integrity in chronic migraine. *J. Headache Pain* **2020**, *21*, 112. [CrossRef]
12. Porcaro, C.; Di Renzo, A.; Tinelli, E.; Di Lorenzo, G.; Seri, S.; Di Lorenzo, C.; Parisi, V.; Caramia, F.; Fiorelli, M.; Di Piero, V.; et al. Hypothalamic structural integrity and temporal complexity of cortical information processing at rest in migraine without aura patients between attacks. *Sci. Rep.* **2021**, *11*, 18701. [CrossRef]
13. Varley, T.F.; Craig, M.; Adapa, R.; Finoia, P.; Williams, G.; Allanson, J.; Pickard, J.; Menon, D.K.; Stamatakis, E.A. Fractal dimension of cortical functional connectivity networks & severity of disorders of consciousness. *PLoS ONE* **2020**, *15*, e0223812. [CrossRef]
14. Moaveninejad, S.; Cauzzo, S.; Porcaro, C. Fractal dimension and clinical neurophysiology fusion to gain a deeper brain signal understanding: A systematic review. *Inf. Fusion* **2025**, *118*, 102936. [CrossRef]
15. Bryce, R.M.; Sprague, K.B. Revisiting detrended fluctuation analysis. *Sci. Rep.* **2012**, *2*, 315. [CrossRef]

16. Hu, K.; Ivanov, P.C.; Chen, Z.; Carpena, P.; Eugene Stanley, H. Effect of trends on detrended fluctuation analysis. *Phys. Rev. E* **2001**, *64*, 011114. [CrossRef] [PubMed]
17. Linkenkaer-Hansen, K.; Nikouline, V.V.; Palva, J.M.; Ilmoniemi, R.J. Long-Range Temporal Correlations and Scaling Behavior in Human Brain Oscillations. *J. Neurosci.* **2001**, *21*, 1370–1377. [CrossRef]
18. He, B.J. Scale-Free Properties of the Functional Magnetic Resonance Imaging Signal during Rest and Task. *J. Neurosci.* **2011**, *31*, 13786–13795. [CrossRef] [PubMed]
19. Expert, P.; Lambiotte, R.; Chialvo, D.R.; Christensen, K.; Jensen, H.J.; Sharp, D.J.; Turkheimer, F. Self-similar correlation function in brain resting-state functional magnetic resonance imaging. *J. R. Soc. Interface* **2011**, *8*, 472–479. [CrossRef]
20. He, B.J. Scale-free brain activity: Past, present, and future. *Trends Cogn. Sci.* **2014**, *18*, 480–487. [CrossRef]
21. Chialvo, D.R. Emergent complex neural dynamics. *Nat. Phys.* **2010**, *6*, 744–750. [CrossRef]
22. Willson, K.; Francis, D.P.; Wensel, R.; Coats, A.J.S.; Parker, K.H. Relationship between detrended fluctuation analysis and spectral analysis of heart-rate variability. *Physiol. Meas.* **2002**, *23*, 385–401. [CrossRef]
23. Zuo, X.-N.; Di Martino, A.; Kelly, C.; Shehzad, Z.E.; Gee, D.G.; Klein, D.F.; Castellanos, F.X.; Biswal, B.B.; Milham, M.P. The oscillating brain: Complex and reliable. *NeuroImage* **2010**, *49*, 1432–1445. [CrossRef]
24. Zappasodi, F.; Marzetti, L.; Olejarczyk, E.; Tecchio, F.; Pizzella, V. Age-Related Changes in Electroencephalographic Signal Complexity. *PLoS ONE* **2015**, *10*, e0141995. [CrossRef]
25. Shafto, M.A.; Tyler, L.K.; Dixon, M.; Taylor, J.R.; Rowe, J.B.; Cusack, R.; Calder, A.J.; Marslen-Wilson, W.D.; Duncan, J.; Dalgleish, T.; et al. The Cambridge Centre for Ageing and Neuroscience (Cam-CAN) study protocol: A cross-sectional, lifespan, multidisciplinary examination of healthy cognitive ageing. *BMC Neurol.* **2014**, *14*, 204. [CrossRef]
26. Calhoun, V.D.; Adali, T.; Pearlson, G.D.; Pekar, J.J. A method for making group inferences from functional MRI data using independent component analysis. *Hum. Brain Mapp.* **2001**, *14*, 140–151. [CrossRef]
27. Griffanti, L.; Douaud, G.; Bijsterbosch, J.; Evangelisti, S.; Alfaro-Almagro, F.; Glasser, M.F.; Duff, E.P.; Fitzgibbon, S.; Westphal, R.; Carone, D.; et al. Hand classification of fMRI ICA noise components. *NeuroImage* **2017**, *154*, 188–205. [CrossRef] [PubMed]
28. Shirer, W.R.; Ryali, S.; Rykhlevskaia, E.; Menon, V.; Greicius, M.D. Decoding Subject-Driven Cognitive States with Whole-Brain Connectivity Patterns. *Cereb. Cortex* **2012**, *22*, 158–165. [CrossRef] [PubMed]
29. Magris, M. Detrended Fluctuation Analysis (DFA). Central File Exchange. [MATLAB]. Available online: https://www.mathworks.com/matlabcentral/fileexchange/67889-detrended-fluctuation-analysis-dfa (accessed on 27 January 2025).
30. Chen, X.; Wang, M.; Zhang, H. The use of classification trees for bioinformatics. *WIREs Data Min. Knowl. Discov.* **2011**, *1*, 55–63. [CrossRef]
31. Zhang, G.-Y.; Zhang, C.-X.; Zhang, J.-S. Out-of-Bag Estimation of the Optimal Hyperparameter in SubBag Ensemble Method. *Commun. Stat.-Simul. Comput.* **2010**, *39*, 1877–1892. [CrossRef]
32. Damoiseaux, J.S.; Beckmann, C.F.; Arigita, E.J.S.; Barkhof, F.; Scheltens, P.; Stam, C.J.; Smith, S.M.; Rombouts, S.A.R.B. Reduced resting-state brain activity in the "default network" in normal aging. *Cereb. Cortex* **2008**, *18*, 1856–1864. [CrossRef] [PubMed]
33. Vlahou, E.L.; Thurm, F.; Kolassa, I.-T.; Schlee, W. Resting-state slow wave power, healthy aging and cognitive performance. *Sci. Rep.* **2014**, *4*, 5101. [CrossRef]
34. Yan, L.; Zhuo, Y.; Wang, B.; Wang, D.J.J. Loss of Coherence of Low Frequency Fluctuations of BOLD FMRI in Visual Cortex of Healthy Aged Subjects. *Open Neuroimaging J.* **2011**, *05*, 105–111. [CrossRef] [PubMed]
35. Guan, S.; Wan, D.; Yang, Y.; Biswal, B. Sources of multifractality of the brain rs-fMRI signal. *Chaos Solitons Fractals* **2022**, *160*, 112222. [CrossRef]
36. Grady, C.; Sarraf, S.; Saverino, C.; Campbell, K. Age differences in the functional interactions among the default, frontoparietal control, and dorsal attention networks. *Neurobiol. Aging* **2016**, *41*, 159–172. [CrossRef] [PubMed]
37. Spreng, R.N.; Stevens, W.D.; Viviano, J.D.; Schacter, D.L. Attenuated anticorrelation between the default and dorsal attention networks with aging: Evidence from task and rest. *Neurobiol. Aging* **2016**, *45*, 149–160. [CrossRef]
38. Hrybouski, S.; Cribben, I.; McGonigle, J.; Olsen, F.; Carter, R.; Seres, P.; Madan, C.R.; Malykhin, N.V. Investigating the effects of healthy cognitive aging on brain functional connectivity using 4.7 T resting-state functional magnetic resonance imaging. *Brain Struct. Funct.* **2021**, *226*, 1067–1098. [CrossRef]
39. Cabeza, R.; Anderson, N.D.; Locantore, J.K.; McIntosh, A.R. Aging Gracefully: Compensatory Brain Activity in High-Performing Older Adults. *NeuroImage* **2002**, *17*, 1394–1402. [CrossRef]

40. Seider, T.R.; Porges, E.C.; Woods, A.J.; Cohen, R.A. An fMRI study of age-associated changes in basic visual discrimination. *Brain Imaging Behav.* **2021**, *15*, 917–929. [CrossRef]
41. Li, Y.; Li, C.; Wu, Q.; Xu, Z.; Kurata, T.; Ohno, S.; Kanazawa, S.; Abe, K.; Wu, J. Decreased resting-state connections within the visuospatial attention-related network in advanced aging. *Neurosci. Lett.* **2015**, *597*, 13–18. [CrossRef] [PubMed]